Predicting and harnessing protein flexibility in the design of species-specific inhibitors of thymidylate synthase[1,2]

Timothy A. Fritz [a], Donatella Tondi [b], Janet S. Finer-Moore [a], M. Paola Costi [b, 3], Robert M. Stroud [a, *]

[a] *Macromolecular Structure Group, Departments of Biochemistry and Biophysics, University of California San Francisco, San Francisco, CA 94143-0448, USA*
[b] *Dipartimento Di Scienze Farmaceutiche, Università degli Studi di Modena e di Reggio Emilia, 183 Via Campi, Modena, Italy*

Abstract

Background: Protein plasticity in response to ligand binding abrogates the notion of a rigid receptor site. Thus, computational docking alone misses important prospective drug design leads. Bacterial-specific inhibitors of an essential enzyme, thymidylate synthase (TS), were developed using a combination of computer-based screening followed by in-parallel synthetic elaboration and enzyme assay [Tondi et al. (1999) Chem. Biol. 6, 319–331]. Specificity was achieved through protein plasticity and despite the very high sequence conservation of the enzyme between species.

Results: The most potent of the inhibitors synthesized, *N,O*-didansyl-L-tyrosine (DDT), binds to *Lactobacillus casei* TS (LcTS) with 35-fold higher affinity and to *Escherichia coli* TS (EcTS) with 24-fold higher affinity than to human TS (hTS). To reveal the molecular basis for this specificity, we have determined the crystal structure of EcTS complexed with DDT and 2′-deoxyuridine-5′-monophosphate (dUMP). The 2.0 Å structure shows that DDT binds to EcTS in a conformation not predicted by molecular docking studies and substantially differently than other TS inhibitors. Binding of DDT is accompanied by large rearrangements of the protein both near and distal to the enzyme's active site with movement of Cα carbons up to 6 Å relative to other

ternary complexes. This protein plasticity results in novel interactions with DDT including the formation of hydrogen bonds and van der Waals interactions to residues conserved in bacterial TS but not hTS and which are hypothesized to account for DDT's specificity. The conformation DDT adopts when bound to EcTS explains the activity of several other LcTS inhibitors synthesized in-parallel with DDT suggesting that DDT binds to the two enzymes in similar orientations.

Conclusions: Dramatic protein rearrangements involving both main and side chain atoms play an important role in the recognition of DDT by EcTS and highlight the importance of incorporating protein plasticity in drug design. The crystal structure of the EcTS/dUMP/DDT complex is a model system to develop more selective TS inhibitors aimed at pathogenic bacterial species. The crystal structure also suggests a general formula for identifying regions of TS and other enzymes that may be treated as flexible to aid in computational methods of drug discovery. © 2001 Elsevier Science B.V. All rights reserved.

Keywords: Enzyme specificity; Protein plasticity; Structure-based drug design; Thymidylate synthase

[1] *Escherichia coli* thymidylate synthase numbering is used unless otherwise noted.
[2] PDB coordinates have been deposited with the RCSB with accession ID: 1JG0.
[3] Also corresponding author.

* Corresponding author.
E-mail addresses: costimp@unimo.it (M.P. Costi), stroud@msg.ucsf.edu (R.M. Stroud).

1. Introduction

Thymidylate synthase (TS) is an essential enzyme for life. It catalyzes the formation of the DNA precursor thymidine-5′-monophosphate from the substrate 2′-deoxyuridine-5′-monophosphate (dUMP) and the cofactor 5,10-methylene-5,6,7,8-tetrahydrofolate (mTHF). Because of its critical function, considerable effort has focused on the design of TS inhibitors for the treatment of cancer [2,3]. Less attention has been directed toward the design of species-specific TS inhibitors aimed at treating diseases caused by bacterial, fungal or opportunistic pathogens. In part, the lack of research may be due to the highly con-

served structure of the TS active site [4] which presents a severe challenge for the design of inhibitors with a therapeutic level of discrimination for pathogen versus human TS (hTS). However, given the rise in antibiotic resistant bacteria [5], the relative host toxicity of treatments for fungal infections and the poor therapies available for the treatment of several opportunistic infections of immunocompromised individuals [6], the successful development of pathogen-specific TS inhibitors may offer an important alternative to current antibiotic, antiparasitic and antifungal medications.

Recently, a strategy to create novel TS inhibitors successfully combined computer-based docking to the folate binding site of TS followed by in-parallel chemical synthetic elaboration and enzyme assay [1]. An initial lead (dansyl hydrazine) was discovered from the Available Chemicals Directory ($\approx 150\,000$ compounds) by application of the program DOCK 3.5 [7,8] to a ternary complex crystal structure of *Lactobacillus casei* TS (LcTS) that was kept rigid during DOCK calculations. A small library of molecules synthesized by introducing various chemical 'modules' to the dansyl hydrazine scaffold was created and assayed for inhibition and specificity. The most potent of the inhibitors in the library, N,O-didansyl-L-tyrosine (DDT), was also the most specific for the bacterial LcTS relative to hTS.

We show that DDT inhibits *Escherichia coli* TS (EcTS) with an affinity similar to its affinity for LcTS suggesting that DDT may interact with residues conserved between the bacterial LcTS and EcTS but not hTS. To understand the mechanism of inhibition and the basis of specificity of DDT we determined the crystal structure of EcTS bound to DDT and dUMP. We chose EcTS rather than LcTS since, unlike LcTS, EcTS readily cocrystallizes in ternary complexes with dUMP and cofactor or cofactor analogs. We show that DDT binds to the active site in a manner unlike that predicted from DOCK studies and induces large rearrangements of residues both within and remote from the active site. These rearrangements result in interactions between DDT and conserved residues in bacterial TS but not hTS, which may explain DDT's specificity. Our results suggest that a combination of structure-based fragment selection combined with experimental elaboration and specificity assays can be an effective path to using protein plasticity for the design of drug leads.

2. Results

2.1. Inhibitor specificity

The synthetic elaboration of dansyl hydrazine (the initial DOCK lead) to O-dansyl-L-tyrosine and finally DDT was reflected by a steady progression of improved inhibitor affinity and specificity for LcTS versus hTS where specificity is defined as the IC_{50} for hTS divided by the

IC_{50} for bacterial TS [1] (Table 1). In contrast, nearly all of the improvement in inhibitor affinity and specificity for EcTS was the result of the single-step transition from O-dansyl-L-tyrosine to DDT with O-dansyl-L-tyrosine showing essentially the same affinity as dansyl hydrazine for EcTS. The final level of specificity of DDT for LcTS was 35 and for EcTS was 24 relative to hTS. Compared to the lead molecule dansyl hydrazine, DDT's specificity represents an improvement of 400- and 800-fold for LcTS and EcTS, respectively. DDT's specificity for EcTS and LcTS is at least 100-fold greater than that of ZD1694 (Table 1), an antifolate recently approved for the treatment of colorectal cancer.
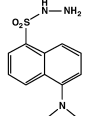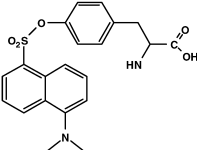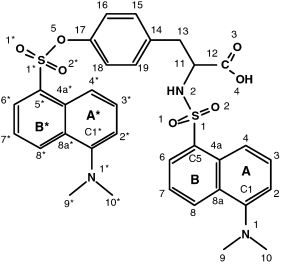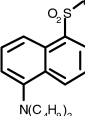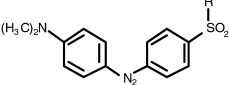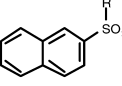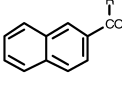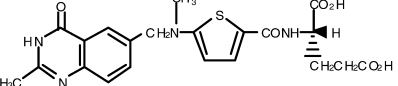
2.2. X-ray crystal structure

The EcTS/dUMP/DDT structure crystallizes as a full physiologic dimer in the asymmetric unit. The crystallographic data and refinement statistics are presented in Table 2. Although the two monomers of the enzyme are structurally unique, the differences between them are minimal and mainly confined to three loop regions consisting of residues 18–23, 81–89 and 103–106. The rms deviation (rmsd) of Cα carbons of the aligned monomers is 0.5 Å. A simulated annealing omit map of the final refined structure shows well defined density for dUMP and DDT in both active sites (Fig. 1). Hydrogen bonds and van der Waals interactions between dUMP and the protein and between DDT and the protein are the same in both active sites. Electron density of the C-terminal isoleucine (Ile 264) was nearly absent so this residue was omitted from the structure as were the side chains of Arg 21 and Arg 107. Because of the structural similarity of the two monomers and bound ligands, detailed analysis for only one of the monomers is presented.

2.3. Binding and orientation of dUMP

Hydrogen bonds and van der Waals interactions to the pyrimidine and ribose rings of dUMP in the EcTS/dUMP/DDT structure are similar to those in other EcTS ternary complexes [9,10]. Despite the preservation of these interactions, dUMP C6 and the active site cysteine (Cys 146) Sγ are separated by > 3 Å which precludes the formation of the covalent bond between these two residues. The creation of this bond represents an early step in the catalytic mechanism of the enzyme. Cys 146 Sγ adopts two conformations, one in which it is hydrogen-bonded to the carbonyl oxygen of Ser 167 and the other in which it is hydrogen-bonded to water 785.

Of four arginine residues of the TS homodimer normally hydrogen-bonded to the phosphate group of dUMP, two (Arg 21A, Arg 166A) are contributed by one monomer and two (Arg 126B, Arg 127B) by the second monomer [9]. In the EcTS/dUMP/DDT structure, only hydrogen bonds from two, Arg 166A and Arg

Table 1
Structures, IC$_{50}$ values and specificities of TS inhibitors

Compound*	IC$_{50}$ (µM) and Specificity Index		
	LcTS	EcTS	hTS
1 Dansyl hydrazine	**458 (0.08)[†]**	**1114 (0.03)**	36
2 O-dansyl-L-tyrosine	**163 (5.0)**	**1170 (0.7)**	771
3 N,O-didansyl-L-tyrosine	**3.4 (35)**	**5.0 (24)**	119
4[‡] 5-dibutylamino-1-naphthylsulfonyl	53	ND[§]	ND
5 4'-(dimethylamino)azobenzene-4-sulfonyl	>> 100	ND	ND
6 2-naphthylsulfonyl	4.7	ND	ND
7 2-naphthylcarbonyl	70	ND	ND
8[¥] ZD1694	**8.8 (0.1)**	**5.3 (0.2)**	0.9

*Atom and ring naming is shown for DDT. [†]Numbers in parentheses are specificity indices defined as the IC$_{50}$ for the human enzyme divided by the IC$_{50}$ for bacterial TS. [‡]For compounds 4–7, the R group (O-dansyl-L-tyrosine for each) is linked via the amine moiety of O-dansyl-L-tyrosine and the data for these compounds were previously reported [1]. [§]ND = not determined. [¥]Data for ZD1694 are from [19].

126B, are preserved. One of the unbound arginines (Arg 21A) is within a loop that has been displaced up to 6 Å from its normal ternary complex location. The other unbound arginine (Arg 127B) lies in two conformations hydrogen-bonded via water molecules to the carbonyl of Leu 138 in one orientation and the amide nitrogen of Ile 129 in the second. The three hydrogen bonds normally contributed to the phosphate by these arginines have been re- placed by water molecules 547, 581 and 590. Hydrogen bonding to the phosphate by an additional residue (Ser 167) is also preserved as in other ternary complexes [10].

2.4. Binding and orientation of DDT

The binding of DDT to EcTS is quite unique and unlike that seen in other ternary EcTS/dUMP/antifolate com-
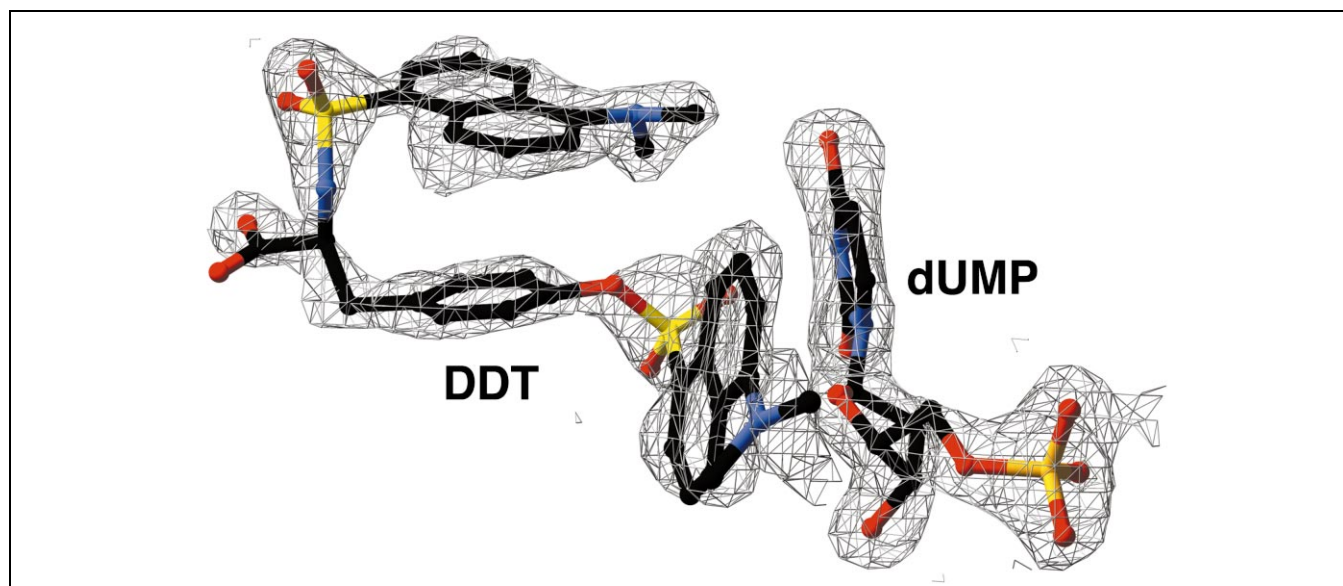
Fig. 1. DDT and dUMP are well defined and oriented in the active site. A simulated annealing $(F_o-F_c)\alpha_{calc}$ omit electron density map was calculated after omitting the ligands from the active site. The refined structures of dUMP and DDT are superimposed on the electron density map which is contoured at 3 sigma. DDT and dUMP are similarly oriented in the second active site.

plexes [9–11]. A comparison of DDT bound to EcTS to the antifolate ZD1694 bound to EcTS and hTS is shown in Fig. 2. The *O*-dansyl moiety of DDT binds to the site normally occupied by the quinazoline group of antifolates (or the pterin ring of cofactor) but in a substantially different orientation. The location of the naphthyl ring of the *O*-dansyl group positions N1* of the dimethyl amino group within 0.2 Å of the site normally occupied by a water molecule (water 580, Fig. 2B) that is critical for mediating the closing of the carboxyl-terminus. In EcTS ternary complexes with cofactor or cofactor analogs this water forms simultaneous hydrogen bonds to a ring nitrogen of the quinazoline group or the natural substrate mTHF and the carbonyl oxygen of the penultimate residue Ala 263 [9,10,12]. The steric bulk of the two methyl groups on N1* of DDT precludes the interaction of DDT

N1* with Ala 263 O and thus keeps the enzyme in an 'open' or apoenzyme-like conformation.

The only direct hydrogen bond between the enzyme and DDT is from non-conserved Thr 78 Oγ1 to DDT O2 (Fig. 2A). All other hydrogen bonds between the enzyme and DDT are mediated via water molecules. DDT O2 forms additional hydrogen bonds to non-conserved Ser 54 Oγ and Thr 78 N via water 549. DDT N1 is hydrogen-bonded to Glu 58 Oε1 via water 440 and DDT N1* forms a hydrogen bond of relatively poor geometry to O5* of dUMP via water 797. Two new water molecules (waters 556 and 737) not present in other EcTS ternary complexes help to stabilize DDT binding by forming aromatic hydrogen bonds to the ligand. Water 556 forms a hydrogen bond between the edge of the A ring of the *O*-naphthyl group and the face of the indole ring of Trp 80 while water 737 forms a hydrogen bond with the face of the A ring of the *O*-naphthyl group and the edge of the A ring of the *N*-dansyl moiety of DDT. A summary of the hydrogen bonds between the protein and DDT is shown in Table 3.

Table 2
X-ray diffraction data and refinement statistics

Resolution (Å)	50–2.0
Unit cell dimensions (Å)	$a = 53.797$, $b = 87.062$, $c = 127.461$
Space group	$P2_12_12_1$
Molecules/asymmetric unit	1
Observed reflections	333 240
Unique reflections	41 069
Completeness	99.6%
R_{merge} (50–2.0 Å)	9.7%
R_{work}	21.2%
R_{free}	25.0%
Total atoms	4848
Water molecules	398
rmsd bonds (Å)	0.009
rmsd angles (°)	1.7
Average *B*-factor	28.6 (33.5 water, 36.0 ligands)

Table 3
DDT hydrogen bonding to EcTS

Protein/dUMP/H$_2$O residue and atoms	DDT atom(s)	Distance(s)[a]
Thr 78 Oγ	O2	3.2
Thr 78 N (Wat 549)	O2	2.9, 2.6
Ser 54 Oγ (Wat 549)	O2	2.9, 2.6
Glu 58 Oε1 (Wat 440)	N1	2.8, 2.9
Trp 80 ring (Wat 556)	A ring	3.5, 4.1
dUMP 05* (Wat 797)	N1*	3.1, 3.0

[a]When two distances are listed, the first distance is from the protein (or dUMP) atom to the water molecule and the second distance is from the water to the DDT atom. Aromatic hydrogen bond distances are taken from the closest point on the aromatic ring to the water molecule.
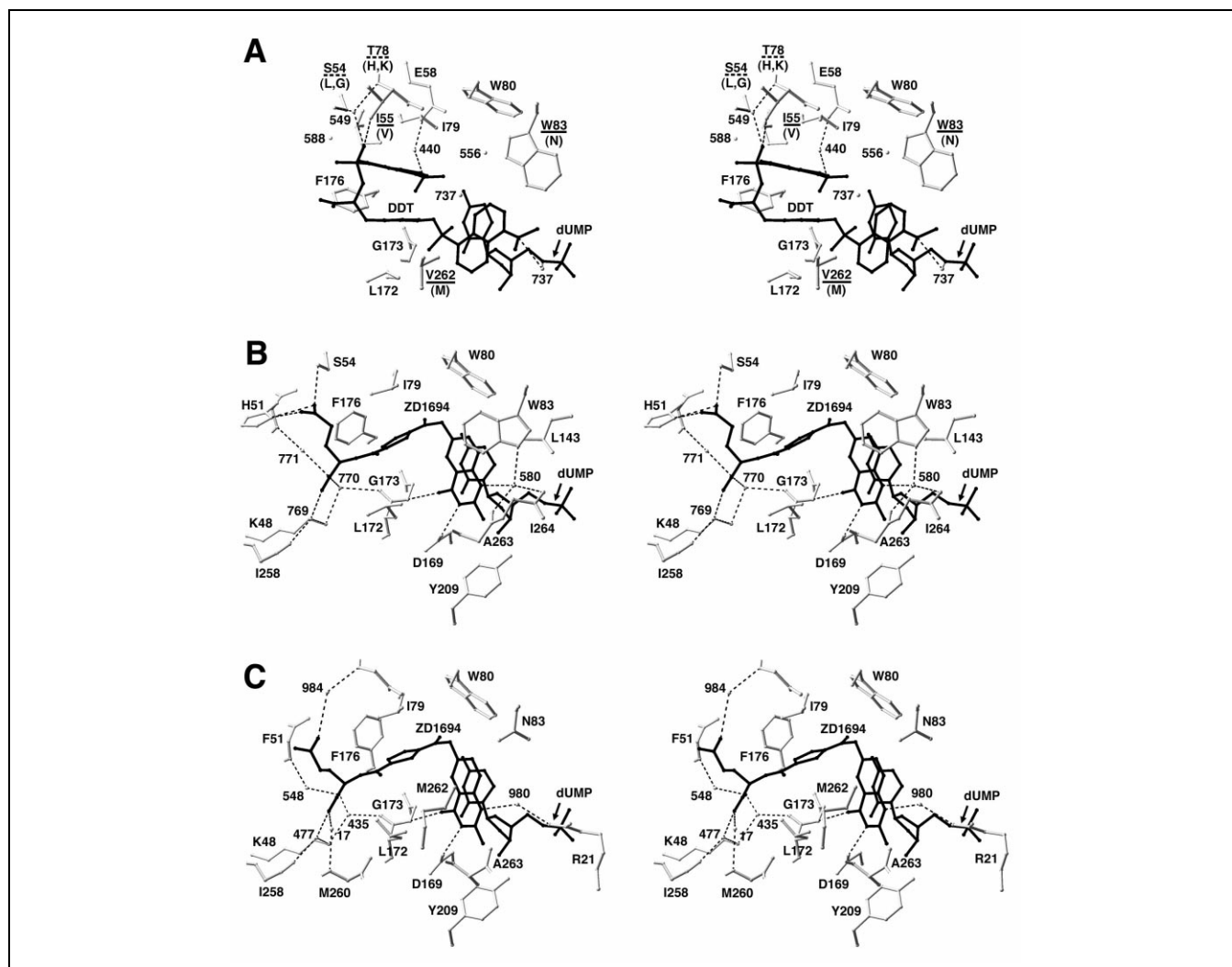
Fig. 2. Conservation and variation of active site protein structure and ligand interactions of EcTS and hTS. Aligned monomers (note the similar orientations of dUMP) of EcTS/dUMP/DDT (A), EcTS/dUMP/ZD1694 (B) and hTS/dUMP/ZD1694 (C) complexes are shown. The full dimeric structures were aligned to each other using the program LSQMAN based upon a core set of residues defined by difference distance matrix analysis [17]. DDT, ZD1694 and dUMP are shown in black and active site residues are shown in gray. Only those portions (backbone or side chain) of protein residues interacting with ligands are shown for clarity purposes. Hydrogen bonds are shown as dashed lines and water molecules are represented by numbers without a single letter prefix. In A, residues contacting DDT which are conserved between EcTS and LcTS (I55, W83 and V262) but which differ from those of hTS are underlined with a solid line and the corresponding hTS residues are shown in parentheses. Residues interacting with DDT which differ between EcTS, LcTS and hTS are underlined with a dashed line and the residues in parentheses indicate the LcTS followed by the hTS residue. All other residues in A are conserved across each of the three TS species. The EcTS numbering system is used in each panel except for waters which retain the numbering of the corresponding structure.

DDT is relatively hydrophobic and the majority of the interactions it forms with EcTS reflect this chemistry. Of the 10 protein residues contacting DDT, seven form purely van der Waals interactions with the ligand (Fig. 3A). The combination of the phenyl ring and *N*-dansyl group of DDT occupy the region of the active site filled by the *p*-aminobenzoic acid (PABA) moiety of antifolates (exemplified by the interactions of the thiophene ring of ZD1694, Fig. 3B). The phenyl ring and A* ring of the *N*-dansyl group form favorable aromatic stacking interactions with each other and, in turn, these rings are sandwiched between the hydrophobic residues Leu 172 and Ile 79. The binding pocket for the phenyl and *N*-dansyl moi-

eties is completed at the bottom of the active site by residues Phe 176 and Ile 55 and at the surface of the active site by Val 262. Phe 176 has swung from its conformation in the folate-bound complex to permit contact of DDT with Ile 55. Ile 55 adopts a conformation not seen in other EcTS ternary complexes to make van der Waals contact with C7 and C8 of the *N*-dansyl group while the DDT phenyl ring forms van der Waals interactions with Val 262. Ile 55 and Val 262 are conserved between EcTS and LcTS but are substituted by Val and Met, respectively, in hTS (Figs. 2A and 3A).

In addition to Ile 55 and Val 262, a third residue that interacts with DDT and is conserved between EcTS and
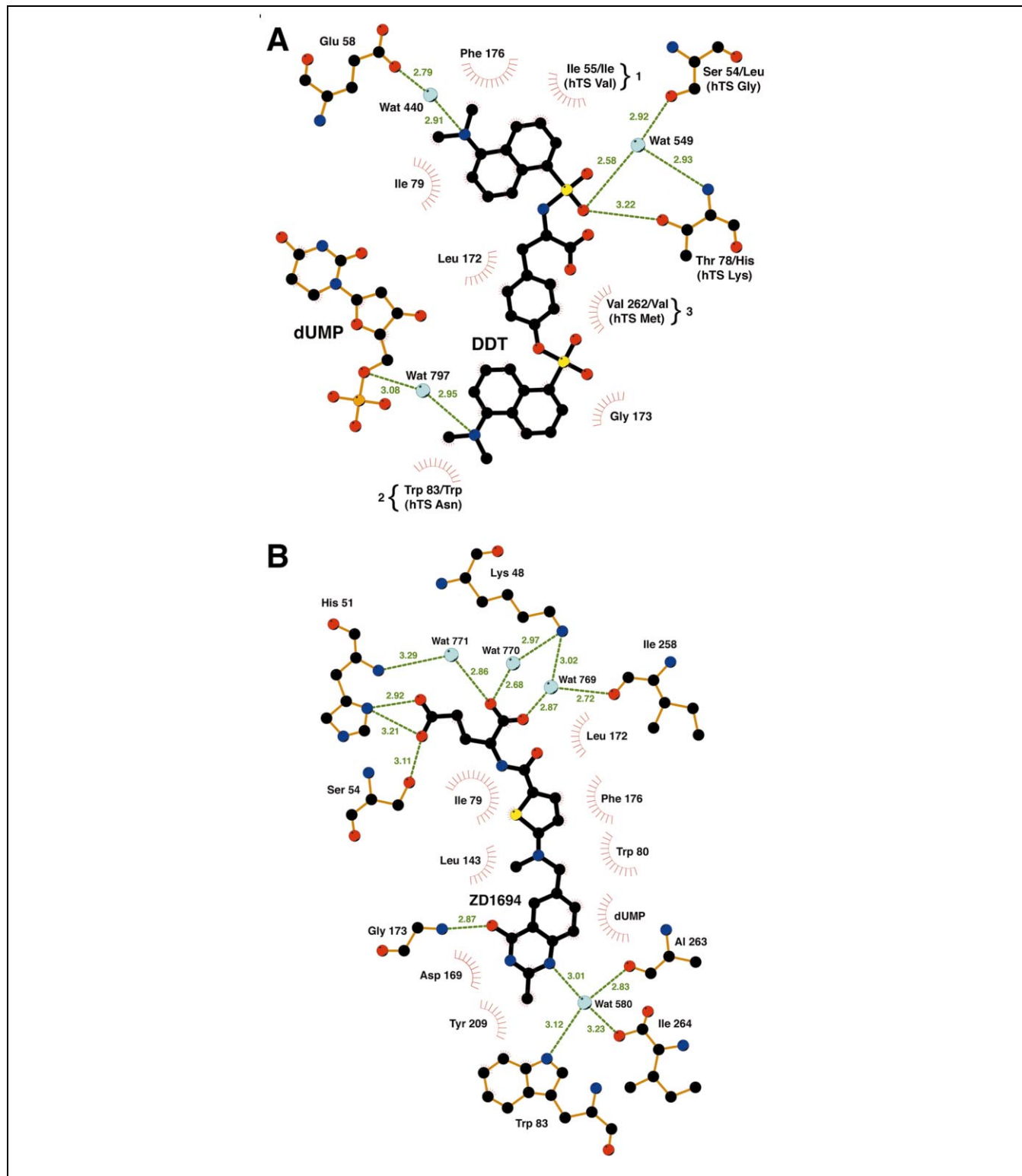
Fig. 3. Schematic diagram comparing the binding to EcTS of DDT (A) and ZD1694 (B). Hydrogen bonds are shown as green dashed lines and hydrophobic interactions are indicated by red 'eyelashes'. In A, non-conserved residues are shown as multiple listings with the first (numbered) being the EcTS residue, the second the LcTS residue and the residue in parentheses the hTS residue. Residues conserved between EcTS and LcTS but not hTS (the 'specificity residues') are indicated by the brackets. Waters are shown in cyan. The figure was generated using the program Ligplot [37].

LcTS but not hTS is Trp 83 (Figs. 2A and 3A). EcTS Trp 83 is Asn in hTS. The DDT C9* methyl group makes van der Waals contact with the side chain of Trp 83 which is rotated by ≈180° relative to other EcTS ternary complexes. The Trp 83 side chain also orients itself to form van der Waals contacts to two other LcTS-specific inhibitors as observed in the crystal structures of these inhibitors in ternary complexes with LcTS [13]. In contrast, the corresponding Asn side chain in hTS ternary complexes forms hydrogen bonds or electrostatic interactions with antifolates. The N1 and N7 atoms of the pyrrolo[2,3-*d*]pyrimidine ring of the antifolate LY231514 form hydrogen bonds to the side chain of this Asn residue (Sayre et al., J. Mol. Biol., in press) while the positive edge potential of the 2-methyl quinazoline ring of ZD1694 interacts with OD1 of the Asn residue [14] (Fig. 2C).

2.5. Comparison of the crystal and modeled structures of DDT binding

A predicted binding mode of DDT to LcTS has been described [1]. Fig. 4 shows a comparison of the docked orientation of LcTS-bound DDT and the crystal structure of DDT bound to EcTS. This comparison is valid since both the current EcTS structure and the LcTS structure used for the modeling [15] are 'open' forms of the enzyme. The rmsd between the two structures for the Cα atoms of the 10 residues interacting with DDT is 1.1 Å. DOCK was roughly successful in its prediction that the *O*-dansyl and phenyl rings of DDT would bind to the regions of the active site normally occupied by the quinazoline and PABA moieties, respectively, of antifolates [1]. However, DDT interacts more deeply in the active site than predicted by DOCK due to the substantial and unanticipated protein rearrangements elicited by DDT binding. The crystal and modeled structures diverge most in the location of the *N*-dansyl moiety. The active site opens up in the region where the *N*-dansyl ring was predicted to bind; consequently DOCK found several high scoring conformations for the *N*-dansyl moiety. The docked orientation of this dansyl group extends away from the active site and many orientations bury this dansyl ring against non-polar surface patches in the LcTS structure, such as that defined by LcTS residues Ala 309 and Ile 310 (EcTS Gly 257 and Ile 258, respectively), and that defined by LcTS residues Leu 56, Ile 81 and the Cβ of His 80 (EcTS Ser 54, Ile 79 and Thr 78, respectively). A more extensive search of DDT conformational space than the 500 structures initially used may have more closely predicted the conformation of DDT bound to EcTS.

It was noted that no single modeled conformation of DDT could explain the structure–activity relationships (SARs) of the other inhibitors synthesized in-parallel with DDT [1]. The orientation of DDT revealed by the crystal structure explains the observed binding affinity of many of these inhibitors, several of which are shown in Table 1. The compound containing a dibutyl amino group in place of the *N*-dansyl dimethyl amino atoms has an IC_{50} at least 15-fold higher than DDT. The crystal structure shows that this hydrophobic dibutyl amino structure would be unfavorably packed into a hydrophilic pocket lined by residues Asn 177, His 147, Glu 58, Ser 180 and the pyrimidine base of dUMP. Inhibitors with bulkier substituents than the *N*-dansyl moiety, such as the 4′-(dimethylamino)azobenzene-4-sulfonyl group, had IC_{50} values at least 15-fold higher than DDT. These larger, hydrophobic groups would have difficulty being accommodated within and, thus, would likely be forced from the active site and exposed to the unfavorable environment of bulk solvent. It was also noted that the docked structures could not explain why sulfonamide compounds always bound better (6–15-fold) than their amide counterparts. The current structure suggests that the substitution of the *N*-dansyl sulfonyl group with a carbonyl would be unfavorable due to the tendency of the amide bond towards planarity. This geometry would again force the amide-linked rings out of the active site, a situation that could not be overcome by torsions about adjacent bonds. Though these inhibitors (including DDT), when bound to LcTS, may adopt dissimilar conformations compared to EcTS-bound DDT, the ability of the crystal structure to explain the SAR of several compounds suggests that the inhibitors do tend to bind in a similar conformation as EcTS-bound DDT with the N-linked ring system (either a single or double ring) stacked above the phenyl ring of DDT.
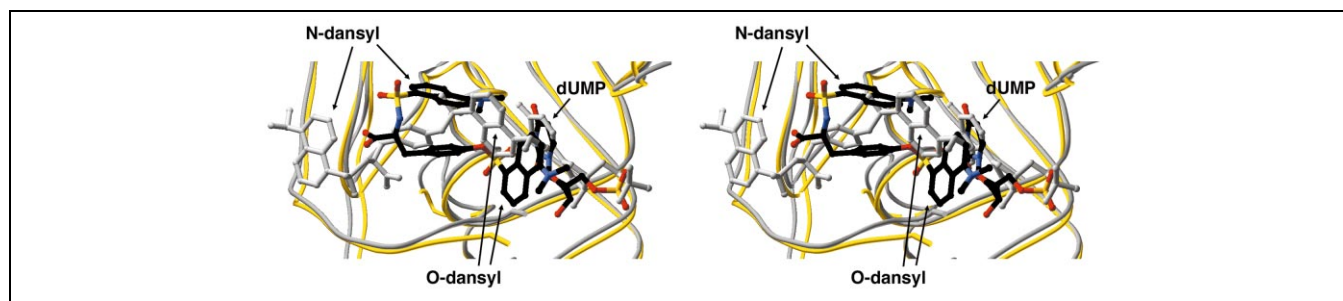

Fig. 4. The crystallographic orientation of DDT bound to EcTS differs from the modeled conformation of DDT bound to LcTS. The LcTS/dUMP/DDT complex is shown in gray and the EcTS/dUMP/DDT complex is shown in yellow (ribbon) and atomic colors (DDT, dUMP).

2.6. Protein plasticity

Many enzymes reorient active site residues to permit the binding of non-native ligands [16]. The conformation adopted by DDT when bound to EcTS presents an unusual structure to be accommodated by the EcTS active site. The active site residue plasticity induced by DDT binding is shown in Fig. 5A. Significant reorientation of
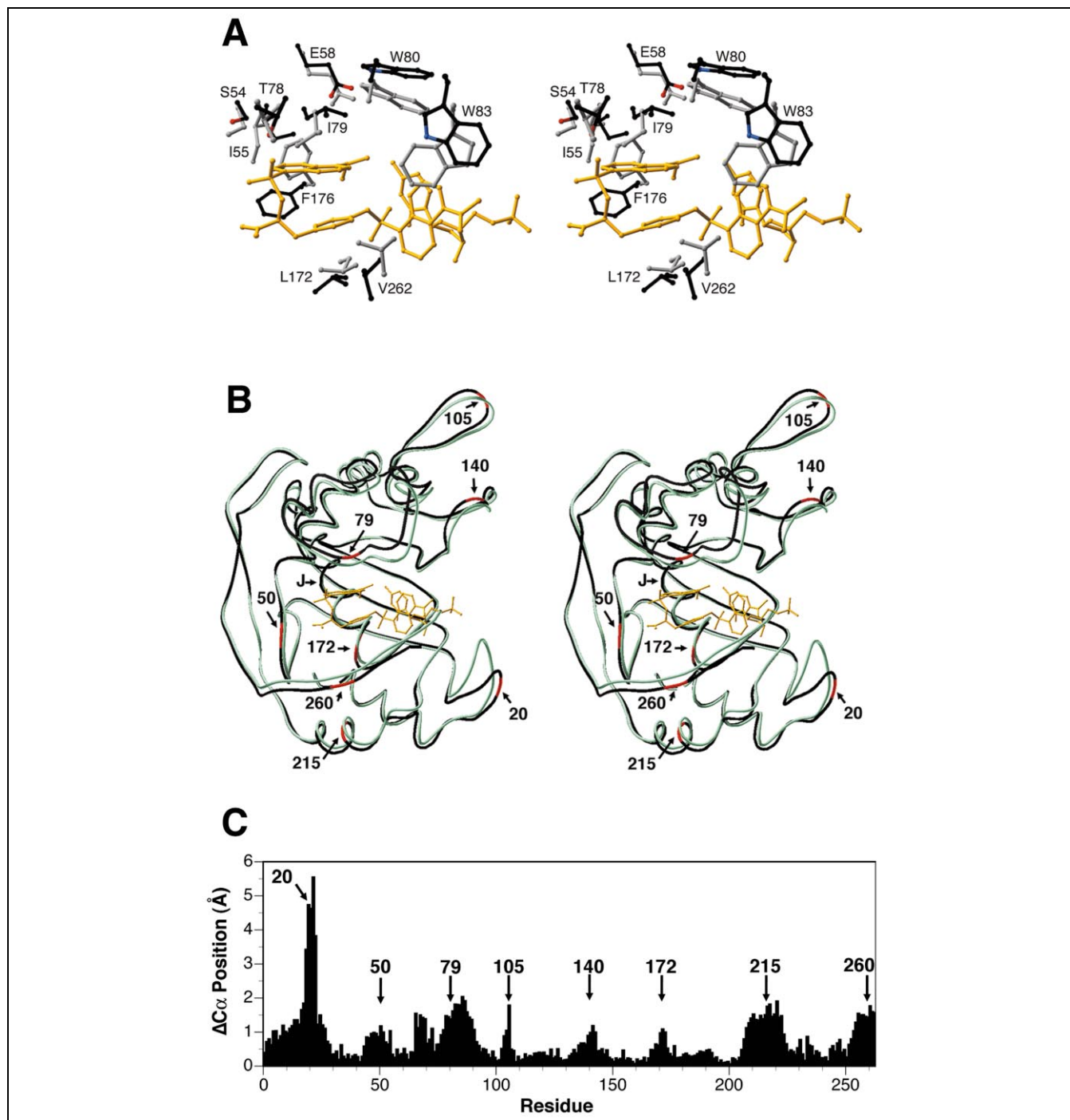

Fig. 5. DDT binding induces dramatic side chain and backbone plasticity. A: Divergent stereo view showing the plasticity of the side chains of active site residues between the EcTS/dUMP/DDT and EcTS/dUMP/ZD1694 structures. DDT and dUMP are shown in yellow, active site residues from the EcTS/dUMP/DDT structure are shown in atomic colors and active site residues from the EcTS/dUMP/ZD1694 structure are shown in gray. B: Divergent stereo view of aligned monomer backbones of the EcTS/dUMP/DDT (black and red) and EcTS/dUMP/ZD1694 (green) structures. The orientation of the structure is the same as that in A and DDT and dUMP are shown in yellow. Residues in red mapped onto the EcTS/dUMP/DDT backbone structure are approximately centrally located residues of protein segments which shift by > 1Å between the two structures. The location of the J-helix (J) is also indicated. C: Difference in Cα position between aligned structures of the EcTS/dUMP/DDT and EcTS/dUMP/ZD1694 complexes with the position of residues shown in B indicated.

the side chains of Ile 55, Thr 78, Ile 79, Trp 83, Leu 172, Phe 176 and Val 262 as well as translational motions of Ser 54, Glu 58 and Trp 80 can be seen relative to the EcTS/dUMP/ZD1694 complex. The rmsd between the EcTS/dUMP/DDT and EcTS/dUMP/ZD1694 structures for all atoms of the active site residues contacting DDT is 2.0 Å.

Several structural elements of EcTS make concerted, segmental movements upon binding cofactor [9]. In addition to active site residues, binding of DDT to EcTS is accompanied by large rearrangements of the protein distal to the active site (Fig. 5B,C) and it is these same protein segments that shift during segmental accommodation (Fig. 6C,D). Thus, DDT has harnessed the protein flexibility inherent in the enzyme's catalytic mechanism. However, the movements evoked by DDT binding are in roughly the opposite direction to those typically observed for ternary complex formation such that the structure of the EcTS/dUMP/DDT complex more resembles the 'open' or apo conformation of EcTS [17] rather than ternary EcTS complexes with antifolates (or cofactor) and dUMP. The opening of the active site is primarily due
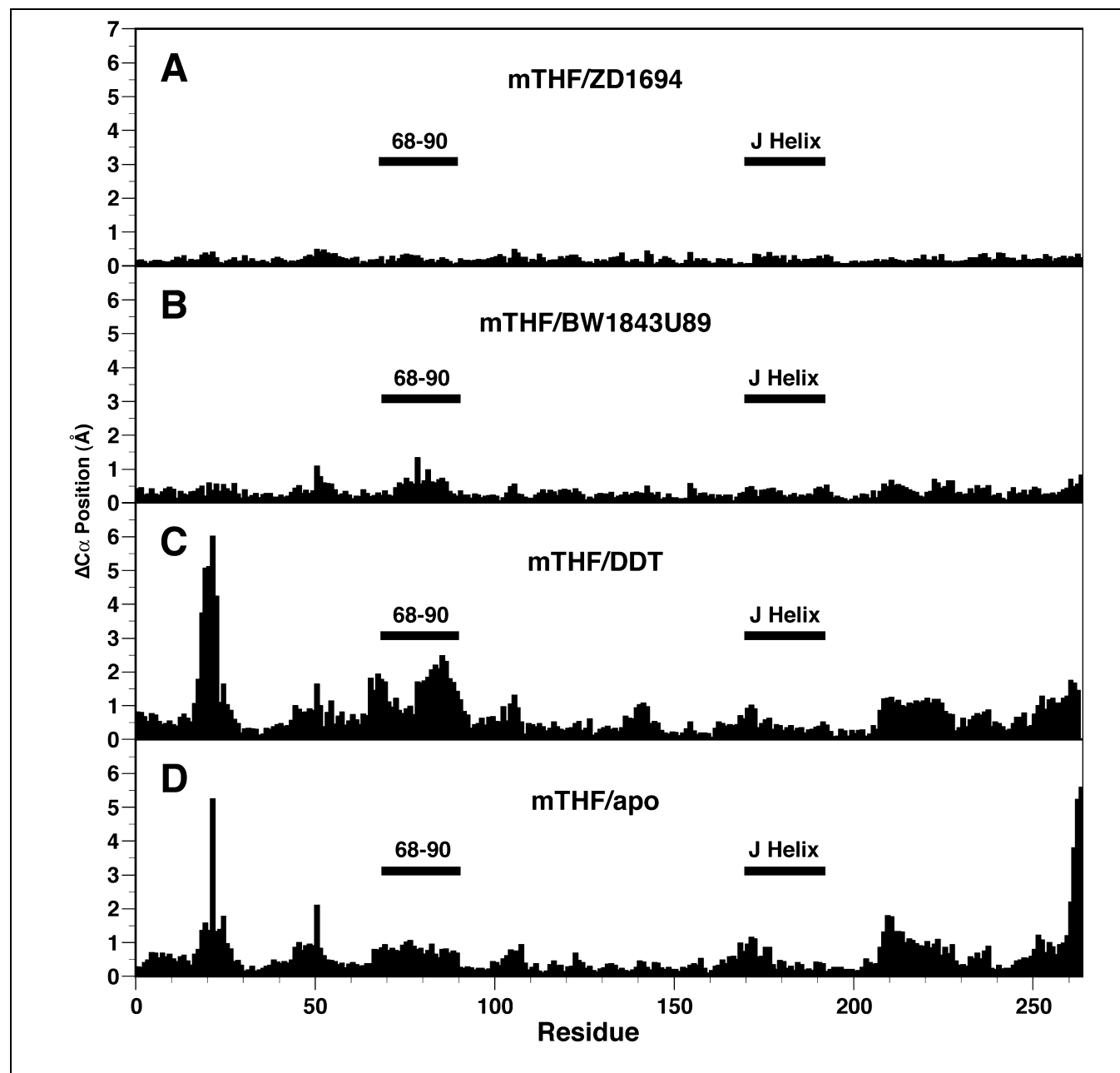
Fig. 6. Ligand-induced, main chain plastic accommodation of EcTS. Individual panels represent the positional difference between corresponding Cα carbons of the EcTS/dUMP/mTHF structure [12] aligned with (A) the EcTS/dUMP/ZD1694 [10], (B) the EcTS/dUMP/BW1843U89 [11], (C) the EcTS/dUMP/DDT or (D) the apo EcTS structure [17]. Only one monomer of each of the aligned structures is shown. D represents the structural changes known as segmental accommodation that take place upon cofactor binding to TS.

to the combination of the phenyl and *N*-dansyl moieties of DDT acting as a wedge between residues Leu 172 and Ile 79 (Fig. 5A). Leucine 172 is at the beginning of the J-helix which is buried at the center of the monomer and forms extensive interactions with 11 distinct protein segments (including three of the five β-sheets which form the dimer interface) that tend to fix the helix in place. Despite these restraining interactions, the Cα of Cys 192 at the C-terminus of the J-helix is shifted by 0.5 Å and the Cα of Leu 172 near the N-terminus of the helix is shifted by 1.1 Å.

Compared to the J-helix, the influence of the phenyl/*N*-dansyl wedge on residues 68–90 is more pronounced since these residues lie at the surface of the enzyme and are less constrained than those of the J-helix. Binding of the antifolate BW1843U89 to EcTS also reorders residues within this region [11,18] but the reorganization caused by DDT is more extensive and results in further distortions of the main chain geometry (Fig. 6B,C). In contrast to the main chain reorganization caused by BW1843U89 and DDT, accommodation by EcTS of the antifolate ZD1694 involves little change relative to the EcTS/dUMP/mTHF structure (Fig. 6A). While the apo EcTS and EcTS/dUMP/DDT ternary structures are more similar to each other than the EcTS/dUMP/DDT complex is to other EcTS ternary structures, substantial differences still remain (Fig. 6C,D).

Shifts in four other protein segments can be understood as a consequence of the effect of the phenyl/*N*-dansyl wedge of DDT upon residues 68–90 and the prevention of the carboxyl-terminus closing by the *O*-dansyl dimethyl amino group (Fig. 5B). Residues 134–148, which include the catalytic Cys 146, shift to maintain their interface with residues 68–90. Similarly, steric clashes with the methyl groups on DDT N1* displace the carboxyl-terminus whose movements are relayed to residues 208–225. In turn, the shift in residues 208–225 is transmitted via main chain hydrogen bonding to residues Gly 25 and Leu 27 in the loop containing Arg 21 whose Cα is displaced by 6 Å from its typical ternary complex location. Residues 208–225 also form hydrogen bonds and van der Waals interactions with Thr 46 and Thr 47 which are at the beginning of a short segment of residues (44–55) containing Ile 55. Thus, the shift in residues 208–225 is responsible for the positioning of Ile 55 and its unique interactions with DDT. In fact, each of the residues conserved between EcTS and LcTS but not hTS (Ile 55, Trp 83 and Val 262) belongs to segments of the protein undergoing substantial reordering resulting from the structural changes evoked by DDT binding.

3. Discussion

3.1. Selectivity of DDT

Protein plasticity increases the probability of developing novel drugs or improving the properties of established ligands by increasing their specificity and/or decreasing their toxicity. A relatively simple approach was used to successfully create TS inhibitors showing a remarkable level (considering the high sequence conservation of TS between species) of specificity for bacterial TS versus hTS [1]. By combining computer-based methods for finding initial leads with in-parallel synthetic elaboration and selectivity assay, a lead molecule, DDT, was designed which displays a 35-fold preference for binding to LcTS relative to hTS and a 24-fold preference for binding to EcTS relative to hTS. In total, fewer than 40 molecules were synthesized leading to DDT. Structural information usefully constrained the diversity available in the synthetic explorations, leading rapidly to more potent inhibitors. Thus, this method avoids the large-scale combinatorial approach in favor of a structure-based, focused library design.

The crystal structure of the EcTS/dUMP/DDT complex suggests that the molecular basis of DDT's bacterial specificity may be achieved primarily from van der Waals contacts with the 'specificity residues' (Ile 55, Trp 83 and Val 262) conserved between EcTS and LcTS but not hTS. Hydrogen bonding to DDT seems unlikely to account for its bacterial specificity since hydrogen bonds to DDT involve either the conserved Glu 58 or residues that differ between EcTS, LcTS and hTS (Ser 54 and Thr 78) (Fig. 2A). Direct evidence that hydrogen bonds do not necessarily promote bacterial specificity comes from the EcTS/dUMP/ZD1694 and hTS/dUMP/ZD1694 structures. Hydrogen bonding of ZD1694 to EcTS and hTS is very similar and involves both EcTS Ser 54 and hTS K78 (Fig. 2B,C) yet ZD1694's affinity for hTS is 6–10-fold greater than for EcTS or LcTS [19]. Four of the seven residues making hydrophobic contact with DDT (Ile 79, Leu 172, Gly 173 and Phe 176) are completely conserved between EcTS, LcTS and hTS and would also seem to offer no obvious mechanism of ligand discrimination between bacterial TS and hTS. Mutational analysis of the 'specificity residues' in EcTS, LcTS and hTS coupled with binding studies may aid in testing this hypothesis.

The argument for the mechanism of specificity assumes that DDT binds in similar orientations to each of the three enzymes. Evidence favoring this hypothesis is the ability of the EcTS-bound conformation of DDT to explain the SAR of dansyl tyrosine derivatives for LcTS as discussed above. Data suggesting that DDT may bind similarly to EcTS and hTS is provided by the crystal structures of EcTS and hTS bound to the antifolates ZD1694 and LY231514. The protein structure corresponding to each of these ligands is remarkably similar (Fig. 2B,C, Sayre et al., J. Mol. Biol., in press) indicating that EcTS and hTS conform to a given ligand in very similar ways. Crystal structures of the LcTS/dUMP/DDT and hTS/dUMP/DDT complexes would resolve the question of whether DDT binds similarly to the three species of TS.

DDT displays similar affinity toward EcTS and LcTS

(Table 1) even though the two enzymes are only 51% identical at the level of primary protein sequence. EcTS shares greater homology with TS from several pathogenic organisms including *Shigella flexneri* (98% identity), *Neisseria gonorrhoeae* (71% identity), *Neisseria meningitidis* (71% identity), *Pseudomonas aeruginosa* (69% identity), and *Mycobacterium tuberculosis* (66% identity). The three 'specificity residues' (Ile 55 Trp 80, Val 262) are conserved among all these species, and all three differ at these positions in hTS. Thus, though EcTS is not itself a drug target, it is likely to be similar enough in structure to serve as an excellent model for TS from these pathogenic organisms. Indeed, the EcTS structure was successfully used as a model for hTS in anticancer drug development efforts at Agouron Pharmaceuticals [20,21].

DDT represents a novel scaffold suitable for further structure-based design of inhibitors that achieve a therapeutic level of specificity for bacterial TS versus hTS. Interactions of DDT with Trp 83 could be optimized by substitution of the naphthyl moiety of the *O*-dansyl group by phenanthrene whose extra ring could form favorable stacking interactions with the Trp 83 side chain. Additionally, a small hydrophobic substituent such as a methyl group attached to the C7 or C8 atoms of the *N*-dansyl ring might improve interactions with Ile 55. The novel water molecule water 737 lies 3.8 Å from DDT C3* and could be displaced by a hydroxyethyl, thioethyl or propanenitrile group (≈ 3.6 Å in length) attached to this atom. One of these chemical moieties placed on DDT C7 might similarly displace the novel water 588 which lies 3.7 Å from this atom. The entropic gain resulting from the displacement of a single bound water molecule typically results in affinity increases of 2–20-fold (0.4–1.8 kcal/mol) [22] so the displacement of three water molecules from the EcTS/dUMP/DDT structure could improve the affinity of DDT for bacterial TS. Whether the release of these waters would increase DDT's specificity in-parallel with any gains in affinity would need to be determined.

3.2. Rules for predicting 'soft spots' on the protein for drug affinity enhancement

The ability to reorient active site residues to accommodate diverse ligands is a characteristic of many proteins [16] and algorithms for including side chain flexibility in computer-based drug design have been described [23,24]. The capacity of an active site to 'flow' around the surface of a novel ligand often involves hydrophobic residues or the hydrophobic areas of polar residues. Within the EcTS active site, the side chains of many of the residues that interact with DDT are substantially reordered relative to their positions in other EcTS ternary complexes (Fig. 5A) and most of these (seven of 10) are hydrophobic. In particular, Ile 55, Ile 79, Trp 83, Leu 172, Phe 176 and Val 262 accommodate DDT binding through a reorientation of side chain atoms. The ability of some of these residues, notably Ile 79, Leu 172 and Phe 176, to reorient in response to ligand binding has previously been found to occur in other ternary complexes of TS [10,11,18,25]. Thus, groups of hydrophobic moieties from residues near to the target site of binding need to be considered as potentially malleable for purposes of drug discovery. We developed an algorithm for selecting an optimized set of these residues, and screening all possible rotamers for a subset that dramatically improves the scoring of drug leads [26].

In addition to side chain reordering, dramatic main chain rearrangements also occur upon DDT binding (Figs. 5B,C and 6C). The main chain of residues 68–90 undergoes some of the most significant movements to accommodate DDT. These residues also shift to accommodate the binding of the antifolate BW1843U89 (Fig. 6B,C), and other antifolates, though they move in different ways. Understanding which regions of a peptide chain will readily move to accommodate ligand binding, and which do not, is key to advancing beyond the 'rigid receptor hypothesis'. The ability to predict the potential manifold of conformers of this segment, for which we have nearly 100 liganded TS structures, can help to identify which regions of other proteins may display plastic properties. Such an algorithm could therefore be important to structure-based lead development that seeks to exploit such accommodating regions.

One measure of protein flexibility used for identifying main chain mobility is the relative magnitude of atomic *B*-factors, as used for example in T4 lysozyme [27]. It was noted that cavity-containing mutants of T4 lysozyme had greatly increased main chain *B*-factors for residues in the F-helix upon binding various 'ligands' within the cavity. However, main chain *B*-factors are not reliable predictors of the flexibility of EcTS residues 68–90 (Table 4). Indeed,

Table 4
EcTS main chain atomic *B*-factors (Å^2)[a]

Complex	Monomer	Residues	
		68–90	Other accessible[b]
EcTS/dUMP/DDT	A	35.0 ± 11.3	35.0 ± 23.9
	B	29.9 ± 11.5	41.6 ± 23.9
EcTS/dUMP/CB3717	A	13.8 ± 4.4	14.2 ± 4.7
	B	26.1 ± 4.0	24.9 ± 6.9
EcTS/dUMP/ZD1694	A	19.5 ± 5.4	21.2 ± 4.3
	B	31.8 ± 5.2	27.8 ± 6.5
EcTS/dUMP/BW1843U89	A	19.5 ± 9.0	17.1 ± 6.6
	B	41.8 ± 5.5	27.7 ± 7.2
EcTS/dUMP/mTHF	A	16.3 ± 5.7	17.6 ± 4.7
	B	32.7 ± 5.5	25.0 ± 7.4
Apo EcTS[c]	A	16.6 ± 4.6	16.0 ± 5.4

[a]Comparison of the average *B*-factors (with standard deviation) of residues 68–90 to residues with similar solvent accessibility of five EcTS ternary complexes [9–12] and apo EcTS [17].
[b]'Other accessible' residues have similar solvent accessibility compared to residues 68–90 and are defined as described in Section 5.
[c]The apo EcTS structure contains a single monomer in the asymmetric unit.

the atomic *B*-factors reflect the amplitude of motion in the protein chain around its energy minimum position, and may not reflect the space or constraints beyond the ∼1 Å amplitude of vibration range. Comparison of the main chain *B*-factors of residues 68–90 to residues with comparable solvent accessibility in three EcTS ternary complexes (EcTS/dUMP/DDT, EcTS/dUMP/CB3717, EcTS/dUMP/ZD1694) and in apo EcTS shows that the *B*-factors for both sets of residues are not significantly different (Table 4). The same is true for the A monomers of the EcTS/dUMP/BW1843U89 and EcTS/dUMP/mTHF structures. Only for the B monomers of these latter two structures are the main chain *B*-factors of residues 68–90 and residues of comparable solvent accessibility significantly different. Ideally, one would want to identify plastic regions from a single crystallographic structure. Therefore, another means of identifying regions of potential protein flexibility for use in drug design is needed.

For the many liganded structures of EcTS, better indicators of plasticity are the presence of few 'scaffolding' hydrogen bonds within and between protein segments, and high solvent accessibility of these segments (Table 5). Here, a protein segment is defined as a covalently contiguous sequence of amino acids of arbitrarily defined length. An inter-segment hydrogen bond is one between the segment and residues outside of it. The 'wedge' of DDT acts between Leu 172 within the J-helix and Ile 79 which lies within the segment comprised of residues 68–90. Why are residues 68–90 able to accommodate DDT while the J-helix remains relatively fixed in place? The J-helix has 80% of its surface area solvent-inaccessible and forms the core of the TS monomer by making contacts with 11 distinct protein segments. These contacts include 14 inter-segment hydrogen bonds (six main chain/main chain, four main chain/side chain and four side chain/side chain) that tend to fix the J-helix in place (Table 5).

In contrast, in the EcTS/dUMP/DDT structure residues 68–90 are mostly devoid of secondary structure and lie at the surface of the enzyme with only 33% of their total surface area buried. Twenty-two of the 23 residues in the 68–90 sequence form no main chain/main chain hydrogen bonds to residues outside this sequence (Table 5). The single residue (Leu 90), which does form an inter-segment

main chain/main chain hydrogen bond, lies at the end ('hinge point') of the sequence and so does little to constrain the movement of the remaining residues. Three residues (Tyr 71, Asn 75, and Trp 80) in 68–90 form inter-segment side chain/main chain or side chain/side chain hydrogen bonds, that remain unbroken between the unliganded and DDT-bound state. These hydrogen bonds may restrict, and so help to define the available motion of the 68–90 sequence. In addition, one hydrogen bond is formed by Asn 76 as DDT binds. Therefore, of the residues in the inaccessible J-helix or those of the segment surrounding and including Ile 79, the latter would be the ones most likely to shift the most upon accommodating a novel ligand. Residues 68–90 form similar numbers and types of hydrogen bonds in the apo EcTS and EcTS/dUMP/ZD1694 structures indicating that the hydrogen bonding of these residues is structure independent. This is important as it shows that these residues could have been identified as being potentially plastic (evidenced by low numbers of inter-segment hydrogen bonds and high solvent accessibility) from any single EcTS structure.

The residues in the F-helix of apo T4 lysozyme are also relatively solvent-accessible (54% buried surface area) and form few inter-segment hydrogen bonds (Table 5). The data in Table 5 suggest that two or fewer main chain/main chain, three or fewer main chain/side chain and two or fewer side chain/side chain hydrogen bonds permit plastic adaptation of protein segments though these numbers may need refinement by analyses of additional protein structures. The short length (eight residues) of the T4 lysozyme F-helix indicates that substantially fewer than the 23 residues of the EcTS 68–90 segment may be capable of plastic adaptation.

Identification of similar core and surface residues that can interact with ligands in the target site on proteins is a key element in identifying protein segments that can be treated as malleable, for the purpose of site directed alterations of a drug lead that would extend beyond the binding site if the site was treated as being relatively rigid. This approach to identify main chain malleability is complementary to, and extends an approach that defines an algorithm for identifying side chains that can reorient to accommodate changes in a drug lead [26].

Table 5
EcTS and T4 lysozyme inter-segment hydrogen bonding

Complex	Residues	Hydrogen bond type and number[a]		
		Main/main	Main/side	Side/side
EcTS/dUMP/DDT	68–90	1	3	2
	J-helix	6	4	4
EcTS/dUMP/ZD1694	68–90	2	2	1
Apo EcTS	68–90	2	3	2
T4 lysozyme	107–113 (F-helix)	2	1	1

[a]Hydrogen bonds between residues 68–90 or the J-helix in the indicated EcTS structures or the F-helix of T4 lysozyme and other protein segments were counted and categorized as either main chain/main chain, main chain/side chain or side chain/side chain.

4. Significance

TS is an anticancer target due to its essential role in DNA biosynthesis, a role which also makes TS an attractive target for species-specific antibacterial, antifungal and antiparasitic drugs that act on these species without inhibiting hTS. However, the high sequence conservation of TS across species makes this goal a significant challenge. We have developed bacterial-specific competitive TS inhibitors using a combination of computer-based screening followed by in-parallel chemical synthesis and specificity assay against a panel of pure TS from bacterial and human species. The most potent and selective of these inhibitors, DDT, binds to bacterial species *L. casei* and *E. coli* TS with 35- and 24-fold higher affinity, respectively, than to hTS. The crystal structure of DDT with EcTS and dUMP suggests that DDT's specificity may derive from van der Waals interactions, not hydrogen bonding, to 'specificity residues' conserved in bacterial TS but not hTS. The conformation DDT adopts when bound to TS is unlike other antifolates and the enzyme accommodates DDT binding by undergoing substantial protein movements relative to other EcTS ternary complexes. These movements occur both near and far from the active site and permit the interaction of DDT with the specificity residues. Examination of the structure suggests that the phenyl and *N*-dansyl groups of DDT act as a wedge between residues Leu 172 and Ile 79 to reorder residues 68–90, a protein domain of TS known to reorder to accommodate ligand binding. The high solvent accessibility and relative scarcity of hydrogen bonds formed between residues 68–90 and the remainder of the protein may account for the plasticity of these residues and suggests that solvent-accessible, ligand-contacting segments of other proteins with few hydrogen bonds (≤7) to the rest of the protein may exhibit plastic properties. The EcTS/dUMP/DDT structure also indicates that targeted modifications to DDT (such as the addition of hydroxyethyl, thioethyl or propanenitrile groups to DDT C3* or C7) to displace active site water molecules may improve DDT's affinity for EcTS and possibly TS of pathogens in which the specificity residues are conserved.

5. Materials and methods

5.1. Enzymology

LcTS [28], EcTS [29] and hTS [30] were expressed and purified as described previously. Purified enzymes were stored at −80°C in 10 mM phosphate buffer (pH 7.0), 0.1 mM EDTA (LcTS, EcTS, hTS) or at −20°C in 20 mM potassium phosphate (pH 7.4), 20 mM β-mercaptoethanol, 5 mM dithiothreitol, 85% saturated ammonium sulfate (EcTS). All enzymes were greater than 95% homogeneous as determined by SDS–PAGE. Kinetic experiments were conducted as previously described [13,31]. Inhibitors were purchased from commercial sources or synthesized as described previously [1].

5.2. Crystallization

EcTS stored at −20°C in 85% saturated ammonium sulfate was dialyzed at 4°C against 20 mM potassium phosphate (pH 8), 2 mM dithiothreitol, 1 mM EDTA before crystallization. Protein solutions were prepared by diluting dialyzed enzyme to 0.26 mg/ml (final concentration) into a solution containing Tris–Cl (10 mM final, pH 8.5), DDT (80 μM final), dUMP (1 mM final) and dithiothreitol (5 mM final). This solution was incubated at 4°C for 30–60 min to allow for ligand binding and then concentrated using a Centricon-30 to a final protein concentration of 6 mg/ml. Well buffer contained 18–20% polyethylene glycol 4000, 0.2 M sodium acetate, 0.1 M Tris–Cl (pH 8.5) and 5 mM dithiothreitol. Protein solutions were mixed with an equal volume of well buffer containing 1 mM dUMP, 80 μM DDT and crystals were grown by hanging drop vapor diffusion over 1 ml of well buffer. Crystals grew in 3–5 days at room temperature. Crystals were soaked in well buffer containing 1 mM dUMP, 80 μM DDT, and 15% ethylene glycol for 2 h and then flash-cooled by plunging into liquid nitrogen. Diffraction intensities were collected at beamline 9-1 at the Stanford Synchrotron Radiation Laboratory. A complete dataset (333 240 total observations) was recorded from a single frozen crystal (60 μm × 60 μm × 500 μm) using 1.0° oscillation images. Intensities from 135 frames were integrated and scaled using the programs DENZO and SCALEPACK [32] in space group $P2_12_12_1$ with unit cell dimensions $a = 53.797$ Å, $b = 87.062$ Å and $c = 127.461$ Å to give 41 069 unique reflections with an overall R_{sym} of 9.7% calculated on intensities.

5.3. Structure solution and refinement

The structure was solved by molecular replacement using the program AMoRe [33] and the reported ternary complex structure of EcTS/dUMP/BW1843U89 [11] with the ligands and water omitted from the model. The EcTS/dUMP/BW1843U89 model gave higher correlation coefficients and lower *R*-factors compared to EcTS/dUMP/CB3717 and EcTS/dUMP/ZD1694 models. Least-squares conjugate gradient minimization followed by grouped *B*-factor minimization using the program CNS [34] gave an *R*-factor of 31.2 ($R_{free} = 35.03$) using all reflections from 50 to 2.0 Å. A difference density electron map (($F_o−F_c)\alpha_{calc}$) calculated following the grouped *B*-factor refinement showed clear electron density for dUMP and DDT in both active sites. DDT and dUMP were modeled into the electron density using the program O [35]. Repeated cycles of conjugate gradient and *B*-factor minimization using CNS along with several trials of simulated annealing and manual rebuilding using O resulted in a final refined structure with an R_{free} of 25.0% and an R_{work} of 21.2% (Table 2).

5.4. Structure analysis

Alignment of proteins was done using the LSQMAN software based upon difference distance matrix plots [17]. The residues (*E. coli* numbering) used for alignment were 32–37, 110–120, 150–160, 180–190 and 197–202. Solvent accessibility was calculated using the program AREAIMOL from the CCP4 suite of programs [36]. Residues of the EcTS/dUMP/DDT complex with similar solvent accessibility to residues 68–90 were defined as

those lying within $\geq$ 5 residue stretches with a buried surface area $\leq$ 50% and consisted of residues 1–24, 99–109 and 212–263.

Acknowledgements

References

[1] D. Tondi, U. Slomczynska, M.P. Costi, D.M. Watterson, S. Ghelli, B.K. Shoichet, Structure-based discovery and in-parallel optimization of novel competitive inhibitors of thymidylate synthase, Chem. Biol. 6 (1999) 319–331.

[2] M.P. Costi, Thymidylate synthase inhibition: a structure-based rationale for drug design, Med. Res. Rev. 18 (1998) 21–42.

[3] R.C. Jackson, Contributions of protein structure-based drug design to cancer chemotherapy, Semin. Oncol. 24 (1997) 164–172.

[4] C.W. Carreras, D.V. Santi, The catalytic mechanism and structure of thymidylate synthase, Annu. Rev. Biochem. 64 (1995) 721–762.

[5] T.M. File Jr., Overview of resistance in the 1990s, Chest 115 (1999) 3S–8S.

[6] R.E. Chaisson, J.E. Gallant, J.C. Keruly, R.D. Moore, Impact of opportunistic disease on survival in patients with HIV infection, Aids 12 (1998) 29–33.

[7] D.M. Lorber, B.K. Shoichet, Flexible ligand docking using conformational ensembles, Protein Sci. 7 (1998) 938–950.

[8] B.K. Shoichet, A.R. Leach, I.D. Kuntz, Ligand solvation in molecular docking, Proteins 34 (1999) 4–16.

[9] W.R. Montfort, K.M. Perry, E.B. Fauman, J.S. Finer-Moore, G.F. Maley, L. Hardy, F. Maley, R.M. Stroud, Structure, multiple site binding, and segmental accommodation in thymidylate synthase on binding dUMP and an anti-folate, Biochemistry 29 (1990) 6964–6977.

[10] E.E. Rutenber, R.M. Stroud, Binding of the anticancer drug ZD1694 to *E. coli* thymidylate synthase: assessing specificity and affinity, Structure 4 (1996) 1317–1324.

[11] T.J. Stout, R.M. Stroud, The complex of the anti-cancer therapeutic, BW1843U89, with thymidylate synthase at 2.0 Å resolution: implications for a new mode of inhibition, Structure 4 (1996) 67–77.

[12] D.C. Hyatt, F. Maley, W.R. Montfort, Use of strain in a stereo-specific catalytic mechanism: crystal structures of *Escherichia coli* thymidylate synthase bound to FdUMP and methylenetetrahydrofolate, Biochemistry 36 (1997) 4585–4594.

[13] T.J. Stout, D. Tondi, M. Rinaldi, D. Barlocco, P. Pecorari, D.V. Santi, I.D. Kuntz, R.M. Stroud, B.K. Shoichet, M.P. Costi, Structure-based design of inhibitors specific for bacterial thymidylate synthase, Biochemistry 38 (1999) 1607–1617.

[14] J. Phan, S. Koli, W. Minor, R.B. Dunlap, S.H. Berger, L. Lebioda, Human thymidylate synthase is in the closed conformation when complexed with dUMP and raltitrexed, an antifolate drug, Biochemistry 40 (2001) 1897–1902.

[15] D.L. Birdsall, J. Finer-Moore, R.M. Stroud, Entropy in bi-substrate

[16] enzymes: proposed role of an alternate site in chaperoning substrate into, and products out of, thymidylate synthase, J. Mol. Biol. 255 (1996) 522–535.

[16] A.M. Davis, S.J. Teague, Hydrogen bonding, hydrophobic interactions, and failure of the rigid receptor hypothesis, Angew. Chem. Int. Ed. 38 (1999) 737–749.

[17] K.M. Perry, E.B. Fauman, J.S. Finer-Moore, W.R. Montfort, G.F. Maley, F. Maley, R.M. Stroud, Plastic adaptation toward mutations in proteins: structural comparison of thymidylate synthases, Proteins 8 (1990) 315–333.

[18] A. Weichsel, W.R. Montfort, Ligand-induced distortion of an active site in thymidylate synthase upon binding anticancer drug 1843U89, Nat. Struct. Biol. 2 (1995) 1095–1101.

[19] A. Gangjee, F. Mavandadi, R.L. Kisliuk, J.J. McGuire, S.F. Queener, 2-Amino-4-oxo-5-substituted-pyrrolo[2,3-*d*]pyrimidines as non-classical antifolate inhibitors of thymidylate synthase, J. Med. Chem. 39 (1996) 4563–4568.

[20] S.H. Reich, M.A. Fuhry, D. Nguyen, M.J. Pino, K.M. Welsh, S. Webber, C.A. Janson, S.R. Jordan, D.A. Matthews, W.W. Smith et al., Design and synthesis of novel 6,7-imidazotetrahydroquinoline inhibitors of thymidylate synthase using iterative protein crystal structure analysis, J. Med. Chem. 35 (1992) 847–858.

[21] M.D. Varney, G.P. Marzoni, C.L. Palmer, J.G. Deal, S. Webber, K.M. Welsh, R.J. Bacquet, C.A. Bartlett, C.A. Morse, C.L. Booth et al., Crystal-structure-based design and synthesis of benz[cd]indole-containing inhibitors of thymidylate synthase, J. Med. Chem. 35 (1992) 663–676.

[22] J.M. Chen, S.L. Xu, Z. Wawrzak, G.S. Basarab, D.B. Jordan, Structure-based design of potent inhibitors of scytalone dehydratase: displacement of a water molecule from the active site, Biochemistry 37 (1998) 17735–17744.

[23] A.R. Leach, Ligand docking to proteins with discrete side-chain flexibility, J. Mol. Biol. 235 (1994) 345–356.

[24] L. Schaffer, G.M. Verkhivker, Predicting structural effects in HIV-1 protease mutant complexes with flexible ligand docking and protein side-chain optimization, Proteins 33 (1998) 295–310.

[25] T.R. Jones, S.E. Webber, M.D. Varney, M.R. Reddy, K.K. Lewis, V. Kathardekar, H. Mazdiyasni, J. Deal, D. Nguyen, K.M. Welsh, S. Webber, A. Johnston, D.A. Matthews, W.W. Smith, C.A. Janson, R.J. Bacquet, E.F. Howland, C.L. Booth, S.M. Herrmann, R.W. Ward, J. White, C.A. Bartlett, C.A. Morse, Structure-based design of substituted diphenyl sulfones and sulfoxides as lipophilic inhibitors of thymidylate synthase, J. Med. Chem. 40 (1997) 677–683.

[26] A.C. Anderson, R.H. O'Neil, T.S. Surti, R.M. Stroud, Approaches to solving the rigid receptor problem by identifying a minimal set of flexible residues during ligand docking, Chem. Biol. 8 (2001) 445–457.

[27] A. Morton, B.W. Matthews, Specificity of ligand binding in a buried nonpolar cavity of T4 lysozyme: linkage of dynamics and structural plasticity, Biochemistry 34 (1995) 8576–8588.

[28] S. Climie, D.V. Santi, Chemical synthesis of the thymidylate synthase gene, Proc. Natl. Acad. Sci. USA 87 (1990) 633–637.

[29] G.F. Maley, F. Maley, Properties of a defined mutant of *Escherichia coli* thymidylate synthase, J. Biol. Chem. 263 (1988) 7620–7627.

[30] V.J. Davisson, W. Sirawaraporn, D.V. Santi, Expression of human thymidylate synthase in *Escherichia coli*, J. Biol. Chem. 264 (1989) 9145–9148.

[31] A.L. Pogolotti Jr., P.V. Danenberg, D.V. Santi, Kinetics and mechanism of interaction of 10-propargyl-5,8-dideazafolate with thymidylate synthase, J. Med. Chem. 29 (1986) 478–482.

[32] Z. Otwinowski, W. Minor, Processing of X-ray diffraction data collected in oscillation mode, Methods Enzymol. 276 (1997) 307–326.

[33] J. Navaza, AMoRe: an automated package for molecular replacement, Acta Crystallogr. A 50 (1994) 157–163.

[34] A.T. Brünger, P.D. Adams, G.M. Clore, W.L. DeLano, P. Gros, R.W. Grosse-Kunstleve, J.S. Jiang, J. Kuszewski, M. Nilges, N.S. Pannu, R.J. Read, L.M. Rice, T. Simonson, G.L. Warren, Crystal-

lography and NMR system: A new software suite for macromolecular structure determination, Acta Crystallogr. D 54 (1998) 905–921.

[35] T.A. Jones, J.Y. Zou, S.W. Cowan, M. Kjeldgaard, Improved methods for binding protein models in electron density maps and the location of errors in these models, Acta Crystallogr. A 47 (1991) 110–119.

[36] S. Bailey, The Ccp4 suite – programs for protein crystallography, Acta Crystallogr. D 50 (1994) 760–763.

[37] A.C. Wallace, R.A. Laskowski, J.M. Thornton, LIGPLOT: a program to generate schematic diagrams of protein–ligand interactions, Protein Eng. 8 (1995) 127–134.